

# GENERALIZED KERNEL-BASED DYNAMIC MODE DECOMPOSITION

Patrick Héas<sup>1,2</sup>, Cédric Herzet<sup>1,2</sup> and Benoit Combès<sup>1,3</sup>

<sup>1</sup>INRIA, <sup>2</sup>IRMAR, <sup>3</sup>IRISA, Univ. Rennes, Campus de Beaulieu, France

## ABSTRACT

Reduced modeling in high-dimensional reproducing kernel Hilbert spaces offers the opportunity to approximate efficiently non-linear dynamics. In this work, we devise an algorithm based on low rank constraint optimization and kernel-based computation that generalizes a recent approach called “kernel-based dynamic mode decomposition”. This new algorithm is characterized by a gain in approximation accuracy, as evidenced by numerical simulations, and in computational complexity.

**Index Terms**— Reduced modeling, kernel-based methods, low-rank approximations, non-linear dynamics

## 1. INTRODUCTION

In this paper, we consider the problem of efficiently approximating trajectories  $x_t(\theta) \in \mathbb{R}^p$ , for different initial conditions  $\theta$  from the following high dimension system:

$$\begin{cases} x_t(\theta) = f_t(x_{t-1}(\theta)), & t = 2, \dots, T, \\ x_1(\theta) = \theta, \end{cases} \quad (1)$$

where  $f_t : \mathbb{R}^p \rightarrow \mathbb{R}^p$  is an arbitrary function whose direct evaluation is time consuming when  $p$  is large.

Dynamic Mode Decomposition [1, 2, 3] is a popular framework for this purpose and relies on efficient linear approximations of the trajectories of (1). It has been extended to the approximation of non-linear behaviors using a decomposition known as extended DMD (EDMD) [4, 5, 6]. Basically, DMD and EDMD are identical, except that the latter first immerses the trajectory through a non-linear mapping  $\Psi$  in a space exhibiting better approximation capabilities. More explicitly, let  $\Psi : \mathbb{R}^p \rightarrow \mathcal{H}$ , where  $\mathcal{H}$  is a Hilbert space endowed with the inner product  $\langle \cdot, \cdot \rangle_{\mathcal{H}}$  and the induced norm  $\| \cdot \|_{\mathcal{H}}$ . EDMD approximates system (1) by:

$$\begin{cases} \eta_t(\theta) = \hat{A}_k \eta_{t-1}(\theta), & t = 2, \dots, T, \\ \eta_1(\theta) = \Psi(\theta), \end{cases} \quad (2)$$

where  $\hat{A}_k : \mathcal{H} \rightarrow \mathcal{H}$  is a linear operator of rank  $\leq k$ , satisfying some optimality criterion (specified later), yielding an approximation of the state  $x_T(\theta)$  by an inverse mapping

$$\tilde{x}_T(\theta) = \Psi^{-1}(\eta_T(\theta)). \quad (3)$$

In this paper, we will focus on reduced models of the form (2)-(3) and where  $\dim(\mathcal{H}) \gg p$  (including  $\dim(\mathcal{H}) = \infty$ ). Such an embedding is appealing due to the ability of high-dimensional Hilbert spaces to linearize differential equations [7, 8, 9]. To obtain a “good” trade-off between accuracy and complexity of the reduced model, one needs to accomplish two challenging tasks: *i*) learn a tractable representation of a low-rank operator  $\hat{A}_k$  yielding an accurate approximation of the form (2)-(3), *ii*) build a low-complexity algorithm to compute  $\tilde{x}_T(\theta)$  satisfying (2)-(3) for a given  $\theta$ .

State-of-the-art methods *e.g.*, [3, 10, 11] involve a complexity in  $\dim(\mathcal{H})$  and thus are non-efficient in high-dimensional settings. In parallel, authors in [5] have introduced an efficient algorithm to compute (3) for any map  $\Psi$  related to a reproducing kernel Hilbert space (RKHS) [12]. This algorithm known as kernel-based DMD (K-DMD) enjoys an advantageous complexity linear in  $p$  and independent of  $\dim(\mathcal{H})$  but relies on restrictive assumptions.

In this work, we propose a new algorithm dubbed “generalized kernel-based DMD (GK-DMD)” that generalizes K-DMD to less restrictive assumptions, while being characterized by a gain in computational complexity and approximation accuracy, as evidenced by our numerical simulations.

## 2. PROBLEM AND EXISTING SOLUTIONS

### 2.1. The Reduced Modeling Problem

Let  $\mathcal{B}(\mathcal{V}, \mathcal{U})$  denote the class of linear bounded operators from  $\mathcal{V}$  to  $\mathcal{U}$  and let  $\mathcal{B}_k(\mathcal{V}, \mathcal{U}) = \{M \in \mathcal{B}(\mathcal{V}, \mathcal{U}) : \text{rank}(M) \leq k\}$ . In this work, we consider a data-driven approach: the reduced model is learnt from a set of representative trajectories  $\{x_t(\vartheta_i)\}_{t=1, i=1}^{T', N}$  of the high-dimensional system corresponding to  $N$  initial conditions  $\{\vartheta_i\}_{i=1}^N$  (with  $T'$  possibly different from  $T$ ). We are interested in the design of an algorithm computing for any  $\theta \in \mathbb{R}^p$  the approximation  $\tilde{x}_T(\theta)$  using a reduced model of the form (2)-(3) and defined as follows.

• **Low-rank operator.** The low-rank linear operator  $\hat{A}_k$  is identified to a solution of the constrained optimization problem

$$A_k^* \in \arg \min_{A \in \mathcal{B}_k(\mathcal{H}, \mathcal{H})} \|\Psi_{\mathbf{Y}} - A\Psi_{\mathbf{X}}\|_{\mathcal{H}\mathcal{S}}, \quad (4)$$

where  $\| \cdot \|_{\mathcal{H}\mathcal{S}}$  refers to the Hilbert-Schmidt norm and where operators  $\Psi_{\mathbf{X}}, \Psi_{\mathbf{Y}} \in \mathcal{B}(\mathbb{R}^m, \mathcal{H})$ , with  $m = N(T' - 1)$ ,

are defined for any  $w \in \mathbb{R}^m$  as the linear combinations  $\Psi_{\mathbf{X}} w = \sum_{i,j=1}^{N,T'-1} \Psi(x_j(\vartheta_i)) w_{(T'-1)(i-1)+j}$  and  $\Psi_{\mathbf{Y}} w = \sum_{i,j=1}^{N,T'-1} \Psi(x_{j+1}(\vartheta_i)) w_{(T'-1)(i-1)+j}$ . These combinations involve the training data set  $\{x_j(\vartheta_i)\}_{i,j=1}^{N,T'}$ , where the  $i$ -th component of a vector is denoted by subscript  $i$ . Operator (4) is a generalization of the solution of the minimization problem in [4, 5], subject to a low-rank constraint as in [1, 2].

• **Minimum distance estimation.** The inverse map (3) is defined as a minimum distance estimate

$$\Psi^{-1}(\eta) \in \arg \min_{z \in \mathbb{R}^p} \|\eta - \Psi(z)\|_{\mathcal{H}}. \quad (5)$$

• **Low-complexity.** The algorithm's complexity is independent of  $\dim(\mathcal{H})$  and the simulated trajectory length  $T$ .

Moreover, in order to enable the independence in  $T$ , we will assume all along this work that  $\mathcal{H}$  is separable and that  $A_k^*$  is diagonalizable. These assumptions enable to evaluate recursion (2) independently of the trajectory length  $T$ . Explicitly, let  $\{\xi_i\}_{i \in \mathbb{N}}$  and  $\{\zeta_i\}_{i \in \mathbb{N}}$  be bases of  $\mathcal{H}$  associated to the left and right eigen-vectors of  $A_k^*$ , *i.e.*,  $\xi_i A_k^* = \lambda_i \xi_i$  and  $A_k^* \zeta_i = \lambda_i \zeta_i$  for  $i \in \mathbb{N}$ , where  $\{\lambda_i\}_{i \in \mathbb{N}}$  is the related sequence of eigen-values sorted by decreasing magnitude. The finite rank of operator  $A_k^*$  and the bi-orthogonality of the left and right eigen-vectors yield  $A_k^* \Psi = \sum_{i=1}^k \lambda_i \langle \xi_i, \Psi \rangle_{\mathcal{H}} \zeta_i$ . Using the notation  $\varphi_i(\theta) = \langle \xi_i, \Psi(\theta) \rangle_{\mathcal{H}}$ , (3) then becomes

$$\tilde{x}_T(\theta) = \Psi^{-1} \left( \sum_{i=1}^k \nu_{i,T} \zeta_i \right), \quad \nu_{i,T} = \lambda_i^{T-1} \varphi_i(\theta). \quad (6)$$

## 2.2. Two Existing Solutions

In the following, we discuss two existing methods which will serve as ingredients for our GK-DMD algorithm.

**Optimal but Intractable.** Reduced model (6) with  $A_k^*$  given by (4) is referred to as *low-rank EDMD*. A generalization of [13, Theorem 4.1] to separable infinite-dimensional Hilbert spaces provides a closed-form expression of operator  $A_k^*$  [14]: a solution of problem (4) for arbitrary value of  $k$  is

$$A_k^* = \mathbb{P}_{\mathbf{Z}^k} \Psi_{\mathbf{Y}} \Psi_{\mathbf{X}}^\dagger, \quad (7)$$

with the orthogonal projector  $\mathbb{P}_{\mathbf{Z}^k} = \hat{P}_k \hat{P}_k^*$ . We use short-hand SVD notations<sup>1</sup> in order to define the operator  $\hat{P}_k \in \mathcal{B}(\mathbb{R}^k, \mathcal{H}) : w \rightarrow \sum_{i=1}^k u_i^{\mathbf{Z}} w_i$  with  $\mathbf{Z} \in \mathcal{B}(\mathbb{R}^m, \mathcal{H})$  as

$$\mathbf{Z} = \Psi_{\mathbf{Y}} \mathbb{P}_{\Psi_{\mathbf{X}}^*}. \quad (8)$$

It can be shown that if  $k \geq m$ , the solution of (4) boils down to the solution of the unconstrained problem [3]  $\hat{A}_k^{\ell s} = \Psi_{\mathbf{Y}} \Psi_{\mathbf{X}}^\dagger$ . However, it remains to propose a tractable algorithm

<sup>1</sup>We will use the short-hand SVD notation for  $M \in \mathcal{B}(\mathcal{V}, \mathcal{U}) : M = U_M \Sigma_M V_M^*$ , where  $U_M \in \mathcal{B}(\mathbb{C}^m, \mathcal{U})$ ,  $\Sigma_M \in \mathcal{B}(\mathbb{R}^m, \mathbb{R}^m)$  and  $V_M^* \in \mathcal{B}(\mathcal{V}, \mathbb{C}^m)$  are defined for any vector  $w \in \mathcal{V}$ ,  $s \in \mathbb{C}^m$  as  $U_M s = \sum_{j=1}^m u_j^M s_j$ ,  $(V_M w)_i = \langle v_i^M, w \rangle_{\mathcal{V}}$  and  $(\Sigma_M s)_i = \sigma_i^M s_i$ .

to build and evaluate reduced model (6) from the closed-form, but potentially infinite-dimensional, solution  $A_k^*$ .

**Tractable but Restrictive.** To tackle the high-dimensional setting  $\dim(\mathcal{H}) \gg p$ , authors propose to consider in their seminal work a specific class of mapping  $\Psi$  from  $\mathbb{R}^p$  to  $\mathcal{H}$  [5]. They assume  $\mathcal{H}$  to be a RKHS [12]. Such a space of functions on  $\mathbb{R}^p$  is uniquely determined by the choice of a symmetric positive definite kernel  $h : \mathbb{R}^p \times \mathbb{R}^p \rightarrow \mathbb{R}$ , such that  $\langle \Psi(z), \Psi(y) \rangle_{\mathcal{H}} = h(y, z)$  with  $z, y \in \mathbb{R}^p$ . The advantage of such a construction is that the kernel trick [15] can be used to compute inner products in the RKHS  $\mathcal{H}$  with a complexity equal to that required for the evaluation of the function  $h$ , which is in general independent of  $\dim(\mathcal{H})$ . More specifically, their method called K-DMD uses the kernel trick to evaluate inner products with eigen-vectors of  $\hat{A}_k^{\ell s}$ . Assuming that the complexity for the evaluation of the kernel is  $\mathcal{O}(p)$ , the overall complexity of the K-DMD algorithm is independent of  $\dim(\mathcal{H})$  and  $T$ , which may be efficient for  $\dim(\mathcal{H}) \gg p$ .

However, as proposed in [5], K-DMD computes an approximation of reduced model (6) under restrictive assumptions. In particular the four following assumptions are needed: *i)*  $A_k^* = \hat{A}_k^{\ell s}$ , *i.e.*, the low-rank constraint in (4) is ignored; *ii)* the operator  $\Psi_{\mathbf{X}}$  is full-rank; *iii)*  $\Psi^{-1}$  is linear; *iv)* the  $\Psi^{-1} \zeta_j$ 's belong to the span of  $\mathbf{Y}$ , where the elements in the set  $\{x_{t+1}(\vartheta_i)\}_{t=1, i=1}^{T'-1, N}$  define the columns  $\{y_i\}_{i=1}^m$  of matrix  $\mathbf{Y} \in \mathbb{R}^{p \times m}$ .

## 3. A GENERALIZED KERNEL-BASED ALGORITHM

### 3.1. The GK-DMD Algorithm

Our generalized kernel-based algorithm, called GK-DMD, is exposed in Algorithm 1. It computes the low-rank reduced model (6) for  $\mathcal{H}$  being an RKHS, with a complexity independent of  $\dim(\mathcal{H})$  and  $T$  and is relieved from the assumptions made in K-DMD. As for K-DMD, the GK-DMD exploits the kernel-trick in step 1) and 6), and resorts to an analogous computation of eigen-functions in step 7). The main innovation in comparison to the latter state-of-the-art algorithm is that GK-DMD computes reduced model (6) based on the exact solution (7) of problem (4). To enable the reduced model to be tractable with the solution (7), GK-DMD relies on the two following original results:

- the right and left eigen-vectors of the optimal operator  $A_k^*$  belong to a low-dimensional sub-space of  $\mathcal{H}$ ; their low-dimensional representations are tractable and computed in steps 1) to 5) relying on the kernel function;
- the inverse map defined in (5) involves a distance minimization problem in  $\mathcal{H}$ ; Taking advantage that, in reduced model (6), the argument of the inverse belongs to a low-dimensional subspace of  $\mathcal{H}$ , the high-dimensional minimization problem boils down to a tractable  $p$ -dimensional optimization problem computed in step 8).

These two results are detailed in Section 3.2.

---

**Algorithm 1 : GK-DMD**


---

• **Off-line. Inputs:**  $x_t(\vartheta_i)$ 's

- 1) Compute matrices  $\Psi_X^* \Psi_X$ ,  $\Psi_Y^* \Psi_Y$ ,  $\Psi_Y^* \Psi_X$  in  $\mathbb{R}^{m \times m}$  with the kernel trick.
- 2) Compute  $(V_{\Psi_X}, \Sigma_{\Psi_X})$  by eigen-decomposition of  $\Psi_X^* \Psi_X$ .
- 3) Compute  $(V_Z, \Sigma_Z)$  by eigen-decomposition of  $Z^* Z$  with  $Z$  given by (8).
- 4) Compute the two matrices given in Proposition 1 and compute their eigen-vector/eigen-value couples  $\{(\tilde{\xi}_i, \tilde{\lambda}_i)\}_{i=1}^k$  and  $\{(\tilde{\zeta}_i, \tilde{\lambda}_i)\}_{i=1}^k$ .
- 5) Rescale  $\tilde{\zeta}_i$ 's so that  $\tilde{\zeta}_i^* E \tilde{\xi}_i = 1$  with  $E = S_k \Psi_Y^* \Psi_X R^*$ .

**Outputs:**  $R, S_k, \tilde{\xi}_i$ 's,  $\tilde{\zeta}_i$ 's and  $\tilde{\lambda}_i$ 's

• **On-line. Inputs:** off-line outputs and  $\theta$

- 6) Compute  $\Psi_X^* \Psi(\theta)$  in  $\mathbb{R}^m$  with the kernel trick.
- 7) Compute eigen-functions  $\{\varphi_i(\theta)\}_{i=1}^k$  defined as

$$\varphi_i(\theta) = \langle \xi_i, \Psi(\theta) \rangle_{\mathcal{H}} = \tilde{\xi}_i^* R \Psi_X^* \Psi(\theta). \quad (9)$$

- 8) Compute  $\tilde{x}_T(\theta)$  solving (10);

**Output:**  $\tilde{x}_T(\theta)$ .

---

Let us meanwhile analyze the advantage of the GK-DMD algorithm in terms of computational complexity. Assuming that the complexity for the evaluation of the kernel is  $\mathcal{O}(p)$ , the overall complexity of the proposed algorithm scales in  $\mathcal{O}(m^2(m+p))$ , just as for K-DMD. We remark that this complexity is independent of  $T$  thanks to the eigen diagonalization of  $A_k^*$ , and independent of  $\dim(\mathcal{H})$  due to the use of the kernel-trick in the first and last steps of the algorithm. Nonetheless, reduced modeling is very concerned by the on-line computational cost, *i.e.*, complexity of computation steps depending on the input  $\theta$ . As  $k \leq m \leq p$  and typically  $k \ll p$ , GK-DMD is attractive by its on-line complexity in  $\mathcal{O}(m^2k + mp)$ , *i.e.*, it scales linearly with respect to the dimension of the reduced model  $k$  or the ambient dimension  $p$ , in comparison to  $\mathcal{O}(m^2p)$  operations for K-DMD. Indeed, the matrix-vector product  $\Psi_X^* \Psi(\theta)$  in step 6) and the inversion in step 8) are both computed in  $\mathcal{O}(pm)$  operations, while eigen-functions in step 7) require  $\mathcal{O}(m^2k)$  operations.

### 3.2. Ingredients for Optimality

In the two next sections, we prove that GK-DMD computes reduced model (6) based on the optimal solution (7) of (4).

#### 3.2.1. Low-Dimensional Representation of $A_k^*$

Steps 1) to 5) of our algorithm rely on the following proposition. Let  $\{\xi_i\}_{i=1}^k$  and  $\{\zeta_i\}_{i=1}^k$  denote the left and right eigen-vectors of  $A_k^*$  associated to its at most  $k$  non-zero eigen-values  $\{\lambda_i\}_{i=1}^k$ .

**Proposition 1** For  $i = 1, \dots, k$ , the left and right eigen-vectors of  $A_k^*$  and its eigen-values satisfy  $\xi_i = U_{\Psi_X} \tilde{\xi}_i$ ,  $\zeta_i = \hat{P}_k \tilde{\zeta}_i$  and  $\lambda_i = \tilde{\lambda}_i$  where  $\{(\tilde{\xi}_i, \tilde{\lambda}_i)\}_{i=1}^k$  and  $\{(\tilde{\zeta}_i, \tilde{\lambda}_i)\}_{i=1}^k$  denote respectively the first  $k$  right eigen-vectors and eigen-values of the matrices  $R \Psi_Y^* \Psi_Y S_k^* S_k \Psi_Y^* \Psi_X R^* \in \mathbb{R}^{m \times m}$

and  $S_k \Psi_Y^* \Psi_Y R^* R \Psi_X^* \Psi_Y S_k^* \in \mathbb{R}^{m \times m}$ , with  $R = \Sigma_{\Psi_X}^\dagger V_{\Psi_X}^*$  and  $S_k = \text{diag}((\sigma_1^Z)^\dagger \dots (\sigma_k^Z)^\dagger 0 \dots 0) V_Z^*$ .

Proposition 1 gives a decomposition of the left eigen-vectors of  $A_k^*$  given in (7). Its proof is detailed in [16]. We deduce from Proposition 1 the closed-form  $i$ -th eigen-function approximation  $\varphi_i(\theta)$  for  $i = 1, \dots, k$  at any point  $\theta \in \mathbb{R}^p$  given in (9). Moreover, this proposition provides a closed-form decomposition for the  $\zeta_i$ 's, the right eigen-vectors of  $A_k^*$  and supplies the related eigen-values. Thanks to Proposition 1, the elements in  $\{(\xi_i, \zeta_i, \lambda_i)\}_{i=1}^k$  issued from the eigen-decomposition of  $A_k^*$  (which correspond to the parameters of reduced model (6)) can be written in terms of their low-dimensional counterpart  $\{(\tilde{\xi}_i, \tilde{\zeta}_i, \tilde{\lambda}_i)\}_{i=1}^k$  efficiently computed in the 5 off-line steps. Note that some simple algebraic calculus show that the normalization of the eigen-vectors is ensured if  $\tilde{\zeta}_i$  is rescaled as  $\tilde{\zeta}_i^* E \tilde{\xi}_i = 1$ , with  $E = S_k \Psi_Y^* \Psi_X R^*$ .

#### 3.2.2. Kernel-Based Inversion

The low-dimensional representation of eigen-vectors of  $A_k^*$  provided in Proposition 1 constitutes the main ingredient of the GK-DMD algorithm. However, to achieve the design of this algorithm, it remains to provide a feasible manner to compute  $\Psi^{-1}$  in (6). Once more, the idea consists in relying on the kernel trick in order to compute the inverse with a complexity independent of  $\dim(\mathcal{H})$ .

Using Proposition 1, we begin by rewriting (6) in terms of  $\tilde{\zeta}_i$ 's,  $\varphi_i(\theta)$ 's and  $\tilde{\lambda}_i$ 's as

$$\tilde{x}_T(\theta) = \Psi^{-1} \left( \sum_{j=1}^k \hat{P}_k \tilde{\zeta}_j \tilde{\lambda}_j^{T-1} \varphi_j(\theta) \right) = \Psi^{-1} (\Psi_Y g^{\theta, T}),$$

with  $g^{\theta, T} = S_k^* (\tilde{\zeta}_1 \dots \tilde{\zeta}_k) \left( \tilde{\lambda}_{\ell, 1}^{T-1} \varphi_1(\theta) \dots \tilde{\lambda}_{\ell, k}^{T-1} \varphi_k(\theta) \right)^*$  in  $\mathbb{R}^m$ . This equation implies the inverse of a linear combination of the  $\Psi(y_i)$ 's, where  $y_i = x_{t+1}(\vartheta_j)$  with  $i = (T' - 1)j + t$  for  $j = 1, \dots, N$  and  $t = 1, \dots, T' - 1$ . From (5), we rewrite the inverse of the linear combination in terms of scalar products in  $\mathcal{H}$  computable using the kernel trick, *i.e.*, given the kernel  $h$ ,

$$\tilde{x}_T(\theta) \in \arg \min_{z \in \mathbb{R}^p} \left( h(z, z) - 2 \sum_{i=1}^m g_i^{\theta, T} h(y_i, z) \right). \quad (10)$$

The minimizer can be computed (up to some accuracy) using standard optimization methods with a complexity independent of  $\dim(\mathcal{H})$ . Moreover, the gradient of the objective is in general closed-form, which enables the use of efficient large-scale optimization techniques such as limited memory quasi-newton methods [17]. In this case, the complexity to compute the inverse is linear in  $p$ .

## 4. NUMERICAL SIMULATIONS

We assess four data-driven reduced modeling methods for the approximation of Rayleigh-Bénard convection [18], which is a standard benchmark model in meteorology. Convection is

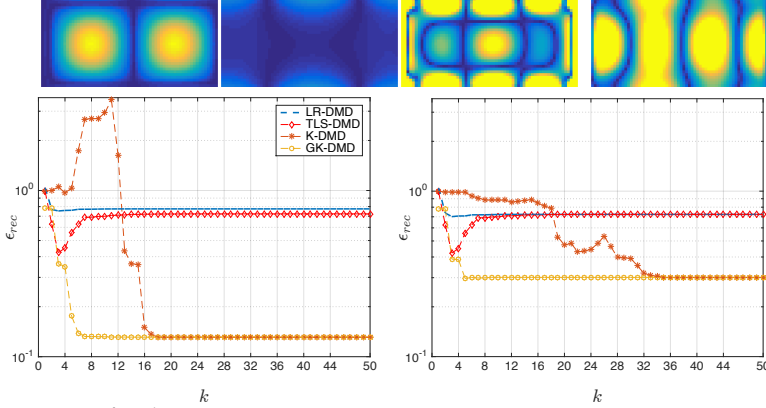


**Fig. 1.** Above: two maps of absolute vorticity (left, colors in the range  $[0, 10^{-3}]$ ) and associated temperature fields (right, colors in the range  $[0, 10^{-6}]$ ) for Rayleigh-Bénard convection. Below: reconstruction error  $\epsilon_{rec}$  as a function of rank  $k$  for GK-DMD and K-DMD with Gaussian (left) and polynomial (right) kernels.

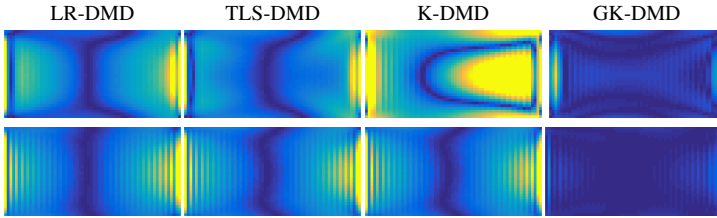


**Fig. 2.** Reconstruction error maps produced for  $k = 5$  (above) and  $k = 15$  (below). Images represent the absolute vorticity (with colors in the range  $[0, 10^{-3}]$ ) of the field  $\tilde{x}_2(\theta) - x_2(\theta)$  for a typical  $\theta$ .

driven by two coupled partial differential equations. After discretisation of these equations, we obtain a discrete system with  $p = 4096$  for the evolution of vorticity and temperature.

The benchmark algorithms are: 1) low-rank DMD (LR-DMD) [13, Algorithm 3], 2) total-least-square DMD (TLS-DMD) [11], 3) kernel-based DMD (K-DMD) [5], 4) the proposed generalized kernel DMD (GK-DMD), *i.e.*, Algorithm 1. For the K-DMD and GK-DMD algorithms, we use a quadratic polynomial kernel or a Gaussian kernel with a standard deviation of 10 [15].

We study the evolution of the reconstruction error  $\epsilon_{rec} = \left( \sum_{j=1}^{N_\theta} \sum_{t=1}^{T-1} \frac{\|\tilde{x}_2(x_t(\theta_j)) - x_{t+1}(\theta_j)\|_2^2}{\|x_{t+1}(\theta_j)\|_2^2} \right)^{1/2}$ , with respect to the rank  $k$ , for a set of initial conditions  $\{\theta_j\}_{j=1}^{N_\theta}$ . It measures the discrepancy between the true state  $x_{t+1}(\theta_j)$  at time  $t + 1$  and the approximated state  $\tilde{x}_2(x_t(\theta_j))$  predicted with the reduced model from the true state at time  $t$ .

The training data of size  $m = 90$  is set as follows: 10 initial conditions  $\vartheta_j$  are sampled from a uniform distribution on an hyper-cube in  $\mathbb{R}^5$  parametrizing solutions of the Lorenz attractor [19]; then using  $\vartheta_j$  to initialize the dynamic model, we compute trajectories for  $t = 1, \dots, 10$  (resulting in 100 states  $x_t(\vartheta_j)$ ). Examples of  $x_t(\vartheta_j)$ 's are displayed in Figure 1. The test data is set as the prolongation of the training data trajectories: the 10 initial conditions are  $\theta_j = x_{10}(\vartheta_j)$

and trajectories  $x_t(\theta_j)$  for  $t = 1, \dots, 10$  are computed in the same way as for the training data set.

We first discuss the results shown in Figure 1 for the Gaussian kernel. Overall, we observe that GK-DMD outperforms almost everywhere the other methods. While K-DMD and GK-DMD perform similarly for  $k \geq 18$ , for  $k < 18$  GK-DMD exhibits a clear gain in accuracy compared to the other methods reaching almost a decade. The gain in accuracy between K-DMD and GK-DMD may be due to the fact that the GK-DMD computes exactly reduced model (6), *i.e.*, considers  $A_k^*$  instead of  $\hat{A}_k^{\ell s}$ . Besides, as  $\text{rank}(\Psi_{\mathbf{X}}^* \Psi_{\mathbf{X}}) = m$ , *i.e.*, operator  $\Psi_{\mathbf{X}}$  is full-rank, a reasonable explanation for the similar performances of the two kernel-based methods in the case where  $k \geq 18$  is that the low-rank constraint becomes inactive (implying that  $\hat{A}_k^{\ell s} = A_k^*$ ),  $\Psi^{-1}$  is well approximated by a linear mapping and furthermore the  $\Psi^{-1}\zeta_j$ 's are well represented in the span of  $\mathbf{Y}$ . A lower value on the accuracy is reached around  $k$  slightly greater than 5, suggesting that only 5 components in  $\mathcal{H}$  can be explained by a linear model. Similar results are obtained with a polynomial kernel. Nevertheless, the gain in accuracy is lower for polynomials, revealing that the reduced model performance is kernel-dependent.

Additionally, the performances of GK-DMD, LR-DMD and TLS-DMD are comparable for  $k < 4$ . Nevertheless, the accuracy of LR-DMD and TLS-DMD reaches a lower bound around  $k \simeq 4$  and then deteriorates as  $k$  increases or reaches an asymptote, suggesting data overfitting.

To complement this quantitative evaluation, we proceed to the visual inspection of the spatial distribution of the error. Typical error maps are shown in Figure 2. It displays the absolute vorticity of the bi-variate error field  $\tilde{x}_2(\theta) - x_2(\theta)$  defined over the bi-dimensional grid, where  $\tilde{x}_2(\theta)$  denotes the approximation provided by the algorithms for a given initial condition  $\theta$ . Error maps are displayed for two values of the dimension  $k$ . The distribution of the error produced by K-DMD reveals that its chaotic behavior as  $k$  increases is caused by errors in a wide range of scales. Error maps of the LR-DMD and TLS-DMD algorithms are very similar. Moreover they seem not to involve significantly as  $k$  increases, except for high frequency revealed at  $k = 15$ . The error maps for GK-DMD show that the decrease in error with respect to  $k$  is related to refinements occurring at increasingly finer scales.

## 5. CONCLUSION

We have presented a new algorithm for the tractable representation of a linear low-rank operator characterizing dynamics embedded in a RKHS. By contrast to existing algorithms, it both exhibits a low computational complexity and requires mild assumptions. Numerical simulations illustrate the gain in accuracy allowed by the proposed algorithm.

## Acknowledgements

This work was supported by the French Agence Nationale de la Recherche through the BECOSE Project.

## 6. REFERENCES

- [1] K. K. Chen, J. H. Tu, and C. W. Rowley, “Variants of dynamic mode decomposition: boundary condition, koopman, and fourier analyses,” *Journal of nonlinear science*, vol. 22, no. 6, pp. 887–915, 2012.
- [2] MR Jovanovic, PJ Schmid, and JW Nichols, “Low-rank and sparse dynamic mode decomposition,” *Center for Turbulence Research Annual Research Briefs*, pp. 139–152, 2012.
- [3] J. H. Tu, C. W. Rowley, D. M. Luchtenburg, S. L. Brunton, and J. N. Kutz, “On dynamic mode decomposition: Theory and applications,” *Journal of Computational Dynamics*, vol. 1, no. 2, pp. 391–421, 2014.
- [4] M. O. Williams, I.G. Kevrekidis, and C.W. Rowley, “A data–driven approximation of the koopman operator: Extending dynamic mode decomposition,” *Journal of Nonlinear Science*, vol. 25, no. 6, pp. 1307–1346, 2015.
- [5] M. O Williams, C. W Rowley, and I. G Kevrekidis, “A kernel-based method for data-driven koopman spectral analysis,” *Journal of Computational Dynamics*, vol. 2, no. 2, pp. 247–265, 2015.
- [6] B. Lusch, J. N. Kutz, and S. L. Brunton, “Deep learning for universal linear embeddings of nonlinear dynamics,” in *Nature Communications*, 2018.
- [7] B. O Koopman, “Hamiltonian systems and transformation in hilbert space,” *Proceedings of the National Academy of Sciences of the United States of America*, vol. 17, no. 5, pp. 315, 1931.
- [8] K. Kowalski and W-H Steeb, *Nonlinear dynamical systems and Carleman linearization*, World Scientific, 1991.
- [9] I. Mezić and A. Banaszuk, “Comparison of systems with complex behavior,” *Physica D: Nonlinear Phenomena*, vol. 197, no. 1-2, pp. 101–133, 2004.
- [10] P. Héas and C. Herzet, “Optimal low-rank dynamic mode decomposition,” in *2017 IEEE International Conference on Acoustics, Speech and Signal Processing (ICASSP)*. IEEE, 2017, pp. 4456–4460.
- [11] M. S. Hemati, C. W. Rowley, E. A. Deem, and L. N. Cattafesta, “De-biasing the dynamic mode decomposition for applied Koopman spectral analysis of noisy datasets,” *Theoretical and Computational Fluid Dynamics*, vol. 31, no. 4, pp. 349–368, 2017.
- [12] I. Steinwart, D. Hush, and C. Scovel, “An explicit description of the reproducing kernel hilbert spaces of gaussian rbf kernels,” *IEEE Transactions on Information Theory*, vol. 52, no. 10, pp. 4635–4643, 2006.
- [13] P. Héas and C. Herzet, “Low rank dynamic mode decomposition: Optimal solution in polynomial time,” *arXiv e-prints*, september 2017.
- [14] P. Héas and C. Herzet, “Low-rank approximation of linear maps,” *arXiv e-prints*, december 2018.
- [15] C. M. Bishop, *Pattern Recognition and Machine Learning (Information Science and Statistics)*, Springer-Verlag, Berlin, Heidelberg, 2006.
- [16] P. Héas, C. Herzet, and B. Combès, “Non-linear reduced modeling by generalized kernel-based dynamic mode decomposition,” *arXiv e-prints*, february 2020.
- [17] J. Nocedal and S. Wright, *Numerical Optimization*, Springer Series in Operations Research and Financial Engineering. Springer New York, 2000.
- [18] S. Chandrasekhar, *Hydrodynamic and hydromagnetic stability*, Courier Corporation, 2013.
- [19] E. N. Lorenz, “Deterministic Nonperiodic Flow.,” *Journal of Atmospheric Sciences*, vol. 20, pp. 130–148, Mar. 1963.